

Electron Landau Damping of Turbulence in the Terrestrial Magnetosheath Plasma

Arya S Afshari¹, Gregory Gershon Howes², Craig A. Kletzing², David Paul Hartley², and Scott A. Boardsen³

¹The University of Iowa

²University of Iowa

³NASA/GSFC-GPHI

November 21, 2022

Abstract

High-quality measurements of electromagnetic fields and electron velocity distributions by the Magnetospheric Multiscale (MMS) mission in Earth's magnetosheath present a unique opportunity to characterize heliospheric plasma turbulence and to determine the mechanisms responsible for its dissipation. We apply the field-particle correlation technique to the MMS measurements to identify the dissipation mechanism and quantify the dissipation rate. It is found that 95% of the intervals have velocity-space signatures of electron Landau damping that are quantitatively consistent with linear kinetic theory for the collisionless damping of kinetic Alfvén waves. About 75% of the intervals have asymmetric signatures, implying that often the collisionless damping is stronger for waves propagating one direction along the magnetic field than the other. Nearly half of the samples have the same electron energization rates as order-of-magnitude estimates of the turbulent energy cascade rate, suggesting that electron Landau damping is frequently responsible for the dissipation of magnetosheath turbulent energy.

Electron Landau Damping of Turbulence in the Terrestrial Magnetosheath Plasma

A. S. Afshari¹, G. G. Howes¹, C. A. Kletzing¹, D. P. Hartley¹, S. A. Boardsen^{2,3}

¹Department of Physics and Astronomy, The University of Iowa, Iowa City, IA USA

²Goddard Planetary Heliophysics Institute, University of Maryland, Baltimore, MD, USA

³NASA/GSFC, Greenbelt, MD, USA

Key Points:

- Of the twenty turbulent magnetosheath intervals analyzed, 95% have velocity-space signatures of electron Landau damping.
- Asymmetric bipolar signatures imply that Landau damping is stronger for waves propagating parallel or anti-parallel to the magnetic field.
- Computed electron energization rates suggest that Landau damping is often a major dissipation mechanism of turbulent magnetosheath energy.

Corresponding author: Arya S. Afshari, arya-afshari@uiowa.edu

Abstract

High-quality measurements of electromagnetic fields and electron velocity distributions by the Magnetospheric Multiscale (MMS) mission in Earth's magnetosheath present a unique opportunity to characterize heliospheric plasma turbulence and to determine the mechanisms responsible for its dissipation. We apply the field-particle correlation technique to the MMS measurements to identify the dissipation mechanism and quantify the dissipation rate. It is found that 95% of the intervals have velocity-space signatures of electron Landau damping that are quantitatively consistent with linear kinetic theory for the collisionless damping of kinetic Alfvén waves. About 75% of the intervals have asymmetric signatures, implying that often the collisionless damping is stronger for waves propagating one direction along the magnetic field than the other. Nearly half of the samples have the same electron energization rates as order-of-magnitude estimates of the turbulent energy cascade rate, suggesting that electron Landau damping is frequently responsible for the dissipation of magnetosheath turbulent energy.

Plain Language Summary

NASA's Magnetospheric Multiscale (MMS) spacecraft pass through the Earth's magnetosheath (the magnetic boundary layer between the Sun's solar wind and the Earth's magnetosphere) on a regular basis. The data from these magnetosheath traversals are analyzed using a novel diagnostic technique. It is found that Landau damping almost always mediates the transfer of energy between turbulent electromagnetic fields and electrons. Landau damping is analogous to a surfer catching a wave, where the surfer (electron) gains energy from the wave (electric field wave), and in the process removes energy from the wave. Compared to the total cascade rate of energy by the turbulence, in half of the intervals studied, Landau damping appears to dominate the dissipation of the turbulence.

1 Introduction

Heliospheric plasma turbulence plays a key role in transferring the energy of large-scale magnetic field and plasma flow fluctuations to smaller scales where their energy can be dissipated, ultimately leading to plasma heating. Expected to play a key role in solar coronal heating (Cranmer et al., 2015), turbulence has been studied using *in situ* measurements in the solar wind (Tu & Marsch, 1995; Bruno & Carbone, 2013; Kiyani et al., 2015) and planetary magnetospheres (von Papen et al., 2014; Hadid et al., 2015; Tao et al., 2015; Ruhunusiri et al., 2017). These studies have shown that the turbulent power spectrum is embedded in the solar wind and changes through interactions with magnetized bodies. Earth's magnetosheath has been shown to exhibit a power law scaling of the power spectral density (PSD) indicative of turbulence (Chasapis et al., 2015; Vörös et al., 2016; Huang et al., 2017). The regions of the magnetosheath downstream from the bowshock, near the magnetopause, provide the conditions to study this turbulence and the turbulent dissipation mechanisms that transfer the energy from the fields to the plasma particles (Huang et al., 2017; Hadid et al., 2018; Chen et al., 2019).

Various turbulent dissipation mechanisms have been proposed to remove energy from the fluctuating fields and inject it into the plasma particles at kinetic scales. Proposed collisionless energy transfer mechanisms include stochastic heating (Johnson & Cheng, 2001; Chandran et al., 2010; Hoppock et al., 2018; Martinović et al., 2020), cyclotron damping (Hollweg & Markovskii, 2002), and Landau damping (Dobrowolny & Torricelli-Ciamponi, 1985; Leamon et al., 1999; Howes et al., 2008; Schekochihin et al., 2009). The resonant field-particle interaction of Landau damping is a viable mechanism by which particles with an appropriate resonant velocity are energized by the parallel electric field of a kinetic Alfvén wave (KAW) (Klein et al., 2017; Howes et al., 2018). A case study by Chen et al. (2019) made the first direct observation of electron Landau damping in magnetosheath turbulence using the Field-Particle Correlation (FPC) technique (Klein & Howes, 2016; Howes et al., 2017; Klein et al., 2017).

Here the Chen et al. (2019) study is built upon by using the FPC technique to analyze twenty intervals of MMS burst-mode data in the Earth's turbulent magnetosheath. The FPC method is used both to identify signatures of the dissipation mechanism in velocity space, as well as to calculate the total energy density dissipation rate. The purpose of this letter is to use these two results from the FPC method to quantify the contribution of electron Landau damping to the total rate of dissipation of the turbulence.

2 Methodology

2.1 The Field Particle Correlation Technique

The FPC technique utilizes the full 3V velocity-space measurements by the MMS spacecraft to generate a *velocity-space signature* that is characteristic of the kinetic mechanism that governs the dissipation of turbulence and consequent energization of particles (Klein & Howes, 2016; Howes et al., 2017; Klein et al., 2017). Collisions may be neglected on the time scale of the collisionless energy transfer that removes energy from the turbulence, so the Vlasov equation for species s describes the plasma dynamics,

$$\frac{\partial f_s}{\partial t} + \mathbf{v} \cdot \nabla f_s + \frac{q_s}{m_s} [\mathbf{E} + \mathbf{v} \times \mathbf{B}] \cdot \frac{\partial f_s}{\partial \mathbf{v}} = 0. \quad (1)$$

The Vlasov equation is multiplied by $m_s v^2/2$ to obtain the time evolution of the 3D-3V phase-space energy density, $w_s(\mathbf{r}, \mathbf{v}, t) = m_s v^2 f_s(\mathbf{r}, \mathbf{v}, t)/2$,

$$\frac{\partial w_s}{\partial t} = -\mathbf{v} \cdot \nabla w_s - q_s \frac{v^2}{2} \mathbf{E} \cdot \frac{\partial f_s}{\partial \mathbf{v}} - q_s \frac{v^2}{2} (\mathbf{v} \times \mathbf{B}) \cdot \frac{\partial f_s}{\partial \mathbf{v}}. \quad (2)$$

When (2) is integrated over all 3D-3V phase-space, yielding the rate of change of total energy \mathcal{W}_s of species s , only the electric field term is non-zero (Howes et al., 2017), so any net change in energy is due to the electric field. Since it is E_{\parallel} that energizes particles in Landau damping, the rate of electron energization by Landau damping can be assessed by taking the unnormalized correlation

$$C_{E_{\parallel}}(\mathbf{v}, t, \tau) = C \left(-q_s \frac{v_{\parallel}^2}{2} \frac{\partial f_e(\mathbf{r}_0, \mathbf{v}, t)}{\partial v_{\parallel}}, E_{\parallel}(\mathbf{r}_0, t) \right). \quad (3)$$

73 The correlation is taken over a sufficiently long interval τ to average out the oscillatory energy
 74 transfer associated with undamped wave motion, exposing the smaller amplitude signal of
 75 secular energization (Klein & Howes, 2016; Howes et al., 2017). Integrating over the velocity-
 76 space dimension perpendicular to the local magnetic field yields the reduced parallel velocity-
 77 space signature $C_{E_{\parallel}}(v_{\parallel}, t, \tau)$.

78 The form of $C_{E_{\parallel}}(v_{\parallel}, t, \tau)$ for Landau damping is illustrated in Figure 1, where (a) the
 79 perturbation of $f(v_{\parallel})$, associated with a KAW travelling up the magnetic field with phase
 80 velocity ω/k_{\parallel} , leads to (b) an instantaneous correlation $C_{E_{\parallel}}(v_{\parallel}, t, 0)$ dominated by oscillatory
 81 energy transfer in time about the resonant phase velocity ω/k_{\parallel} (vertical dashed black line). By
 82 taking the average over a sufficiently long correlation interval, here equal to the wave period
 83 $\tau = T$, $C_{E_{\parallel}}(v_{\parallel}, t, \tau)$ becomes steady in time, and (d) its time average yields the characteristic
 84 bipolar form of the velocity-space signature for Landau damping, where $C_{E_{\parallel}}(v_{\parallel})$ crosses
 85 from negative to positive at the resonant velocity (Klein & Howes, 2016; Howes et al., 2017;
 86 Howes, 2017; Klein et al., 2017; Howes et al., 2018; Klein et al., 2020). Physically, the net
 87 effect of the resonant interaction with E_{\parallel} is that particles with $v_{\parallel} < \omega/k_{\parallel}$ are accelerated to
 88 $v_{\parallel} > \omega/k_{\parallel}$, leading to a net loss of phase-energy density below, and an increase above, the
 89 resonance. This leads to the bipolar velocity-space signature seen in Figure 1(d).

To avoid difficulties with taking velocity-space derivatives in 3V velocity-space, the
 procedure of Chen et al. (2019) is followed and the alternative correlation $C'_{E_{\parallel}}(\mathbf{v}, t, \tau) =$
 $C(q_e v_{\parallel} f_e, E_{\parallel})$ in 3V space is calculated. After integration of $C'_{E_{\parallel}}$ over the perpendicular
 velocity coordinates, $C_{E_{\parallel}}(v_{\parallel})$ is obtained by computing

$$C_{E_{\parallel}}(v_{\parallel}) = -\frac{v_{\parallel}}{2} \frac{\partial C'_{E_{\parallel}}(v_{\parallel})}{\partial v_{\parallel}} + \frac{C'_{E_{\parallel}}(v_{\parallel})}{2}. \quad (4)$$

90 2.2 Selection of Intervals

91 MMS magnetosheath intervals are identified through the use of the orbit plots, Fluxgate
 92 Magnetometer (FGM) data (Russell et al., 2016), and Fast Plasma Investigation (FPI) density

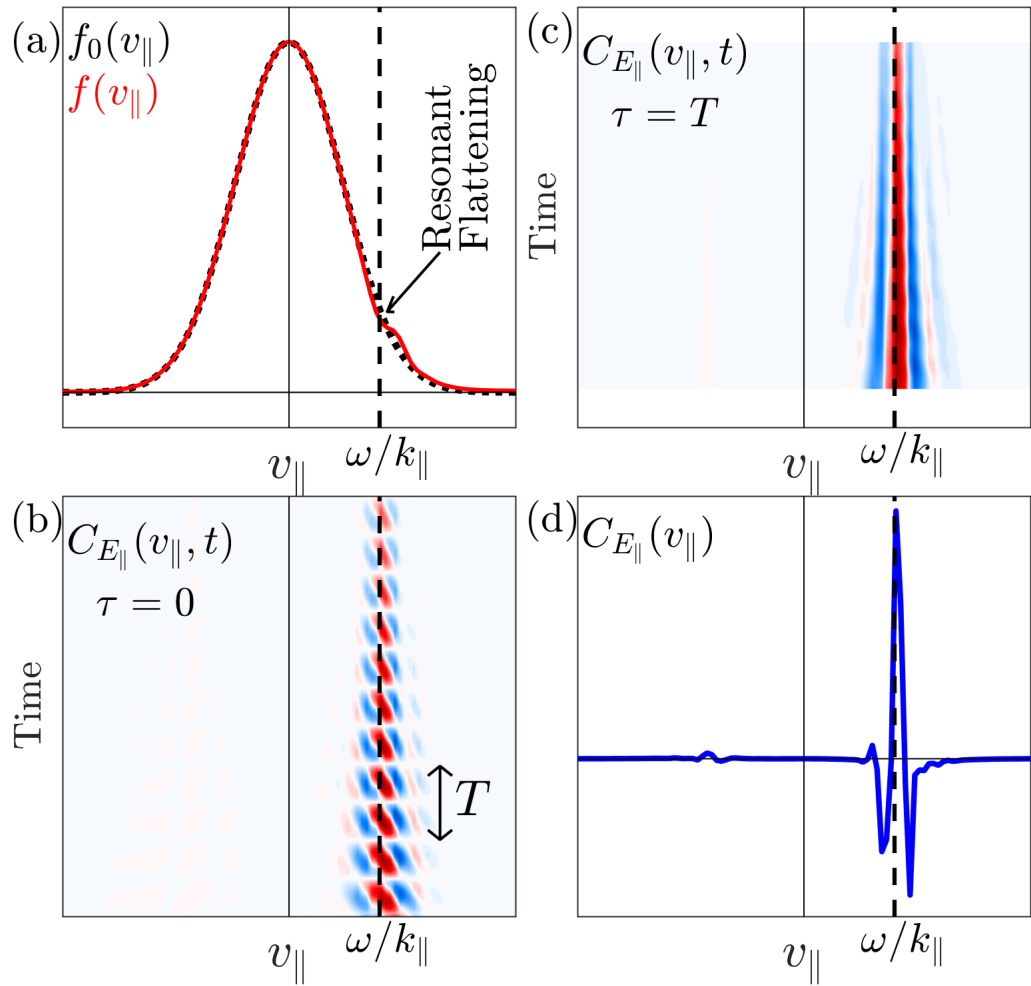


Figure 1: (a) Landau damping leads to a flattening of the velocity distribution $f(v_{\parallel})$ at the resonant phase velocity $v_{\parallel} = \omega/k_{\parallel}$. (b) An instantaneous field-particle correlation with $\tau = 0$ yields a signature in v_{\parallel} that oscillates in time. (c) Averaging over an interval equal to the wave period $\tau = T$ leads to a persistent velocity-space signature. (d) The time-averaged correlation $C_{E_{\parallel}}(v_{\parallel})$ exhibits a bipolar signature, crossing from negative to positive at the resonant velocity, a distinguishing characteristic of Landau damping.

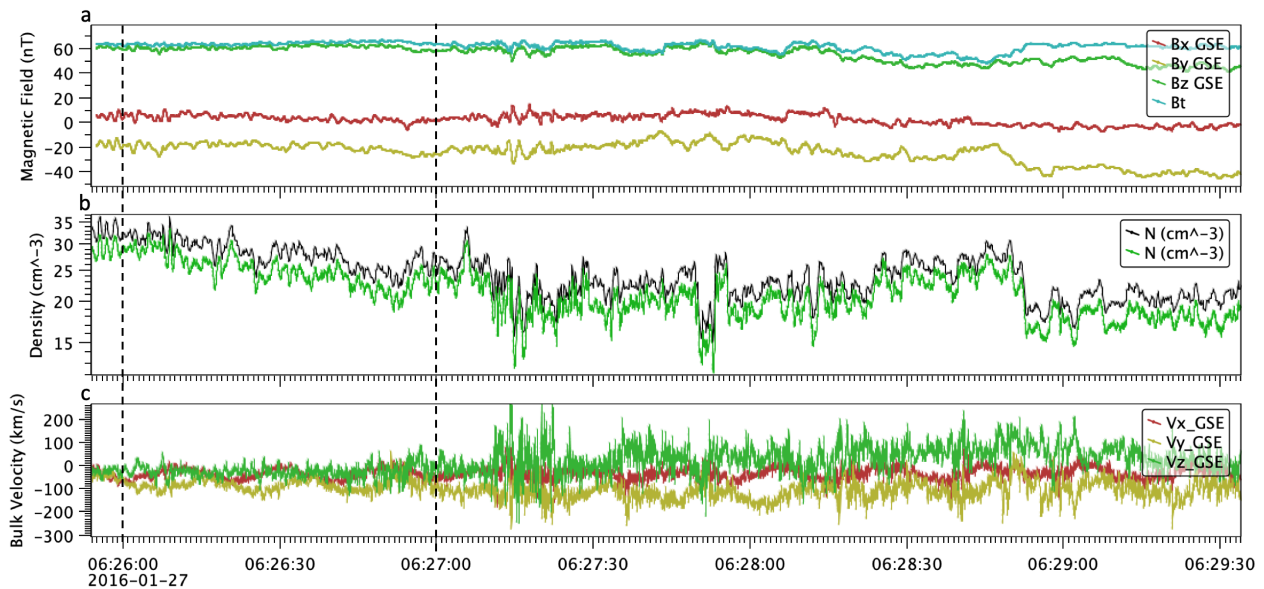


Figure 2: Interval during 2016-01-27 from MMS 1: (a) The magnetic field in geocentric-solar-ecliptic (GSE) coordinates, (b) the ion (black) and electron (green) densities from FPI moments, and (c) the electron bulk velocity.

93 data (Pollock et al., 2016). The magnetosheath is defined as the layer between the bowshock
 94 and the magnetopause, with generally higher temperatures and higher densities than the solar
 95 wind and magnetospheric plasmas. Intervals when MMS is downstream of the bowshock,
 96 close to the magnetopause, are selected. Time-averaging over the correlation interval τ in
 97 magnetic field-aligned coordinates (v_{\parallel} , v_{\perp}) requires an accurate definition of the equilibrium
 98 magnetic field \mathbf{B}_0 . This is facilitated when the magnetic field direction is relatively constant
 99 with no discontinuities. Magnetosheath intervals with relatively constant magnetic field di-
 100 rection, electron density, and ion density, as well as no velocity shears are selected. Figure 2
 101 shows a representation of a burst mode interval from the MMS 1 spacecraft during 2016-
 102 01-27 at 06:25:54 that satisfies the selection criteria, taken on an inbound pass, closer to the
 103 magnetopause than the bowshock. We analyze the $T = 60$ s interval from 06:26:00–06:27:00
 104 (sample 17 in this study) because it contains (a) a steady ambient field, (b) a density typical
 105 of the magnetosheath, and (c) no velocity shears.

2.3 Data Analysis

The MMS measurements employed here are the electron velocity distributions and moments from FPI with a 30 ms cadence (Pollock et al., 2016), the electric field double probes measurements sampled at 8192 Hz (Ergun et al., 2016; Lindqvist et al., 2016), and FGM magnetic field measurements sampled at 128 Hz (Ergun et al., 2016). We follow the same FPC analysis procedure as outlined by Chen et al. (2019). The equilibrium magnetic field is calculated by averaging over the full sample duration T , $\mathbf{B}_0 = \langle \mathbf{B} \rangle_T$. Velocity measurements are transformed to the frame of the mean electron bulk flow, $\mathbf{U}_{0e} = \langle \mathbf{U}_e \rangle_T$, with corrections applied in the energy bins to account for any acceleration due to the charged spacecraft. The velocity coordinates are then projected onto a field-aligned coordinate system, $(v_{\parallel}, v_{\perp})$. Electric field measurements are Lorentz transformed (Chen et al., 2011; Howes et al., 2014) to the same frame, downsampled to 30 ms to match the cadence of FPI, then projected onto \mathbf{B}_0 to obtain $E_{\parallel}(t)$.

To accentuate the signal of secular electron energization using the FPC method, two measures are taken. First, to suppress the large-amplitude signal of oscillatory energy transfer by large-scale electric fields, $E_{\parallel}(t)$ is high pass filtered at 1 Hz to obtain $\overline{E}_{\parallel}(t)$. Second, to eliminate the contribution to $\partial w_e / \partial t$ associated with the equilibrium electron velocity distribution, $f_0(v_{\parallel}, v_{\perp}) = \langle f(v_{\parallel}, v_{\perp}, t) \rangle_T$, which integrates to zero over velocity (Howes et al., 2017), we compute $C'_{E_{\parallel}}(v_{\parallel}, v_{\perp}, t, \tau)$ using the perturbed velocity distribution $\delta f(v_{\parallel}, v_{\perp}, t) = f(v_{\parallel}, v_{\perp}, t) - f_0(v_{\parallel}, v_{\perp})$ (Chen et al., 2019). The resulting correlation $C'_{E_{\parallel}}(v_{\parallel}, v_{\perp}, t, \tau) = C(q_e v_{\parallel} \delta f, \overline{E}_{\parallel})$ is then integrated over the perpendicular velocity coordinates and the azimuthal angle (ϕ) with respect to \mathbf{B}_0 to obtain

$$C'_{E_{\parallel}}(v_{\parallel}, t, \tau) = \int dv_{\perp} \int_0^{2\pi} v_{\perp} d\phi C'_{E_{\parallel}}(v_{\parallel}, v_{\perp}, t, \tau). \quad (5)$$

Finally, (4) is used to obtain the final reduced parallel correlation $C_{E_{\parallel}}(v_{\parallel}, t, \tau)$, from which the velocity-space signature of electron Landau damping as a function of time t and correlation interval τ is sought. In addition, one may integrate $C_{E_{\parallel}}(v_{\parallel}, t, \tau)$ over parallel velocity to

Sample	Date	Interval	τ (s)	Electron β	Ion β	Signature	Electron Energization Rate ($\times 10^{-12} \text{ J m}^{-3} \text{ s}^{-1}$)	Theoretical Cascade Rate ($\times 10^{-12} \text{ J m}^{-3} \text{ s}^{-1}$)	Ratio
00	2015-10-16	09:24:11 - 09:25:21	70	0.08	0.83	S	5.8	2.6	2.2
02	2016-01-12	07:24:38 - 07:25:45	77	0.05	0.75	A	1.7	23	0.075
03	2016-01-13	04:56:40 - 04:57:07	27	0.13	1.12	A	0.42	43	0.0099
04	2016-01-14	05:30:26 - 05:30:51	24	0.15	1.14	A	3.6	33	0.11
05	2016-01-15	02:29:52 - 02:31:10	78	0.62	4.26	S	1.5	4.4	0.33
06	2016-01-16	07:12:20 - 07:13:00	40	0.14	1.11	A	14	30	0.48
07	2016-01-17	01:46:28 - 01:46:43	15	0.11	0.64	A	1.0	34	0.031
08	2016-01-18	00:50:55 - 00:51:57	62	0.17	0.87	A	17	16	1.1
09	2016-01-19	07:24:20 - 07:24:40	20	0.85	5.21	N	1.9	31	0.060
10	2016-01-20	02:52:00 - 02:54:30	150	0.32	0.99	A	0.65	28	0.023
11	2016-01-21	03:51:45 - 03:52:17	32	0.60	2.10	A	0.79	15	0.051
12	2016-01-22	00:19:15 - 00:19:54	39	1.20	8.67	A	1.5	9.3	0.16
13	2016-01-23	02:08:20 - 02:09:42	82	0.77	4.19	A	2.5	33	0.077
14	2016-01-24	04:29:54 - 04:30:43	49	0.25	1.69	A	1.3	5.1	0.26
15	2016-01-25	02:18:00 - 02:18:20	20	0.45	2.38	A	23	28	0.82
16	2016-01-26	00:34:25 - 00:34:45	20	0.21	1.41	S	1.8	8.1	0.23
17	2016-01-27	06:26:00 - 06:27:00	60	0.04	0.34	S	7.6	9.0	0.85
18	2016-01-28	06:05:15 - 06:05:47	32	0.10	0.63	S	52	350	0.15
19	2016-01-29	23:55:15 - 23:55:40	25	0.16	1.55	S	14	49	0.28
20	2016-01-30	03:33:00 - 03:34:10	70	0.04	0.40	A	0.12	1.4	0.090

Table 1: Table of analyzed MMS intervals (all from MMS 1, except for sample 00 from MMS 3), including electron energization rates $\partial W_e / \partial t$ from the integrated experimental measurements and the theoretically estimated turbulent cascade rate ϵ . Qualitative signatures are symmetric (S), asymmetric (A), or no clear signature (N). The Ratio column gives $(\partial W_e / \partial t) / \epsilon$.

122 obtain the rate of change of spatial energy density W_e due to E_{\parallel} at the spacecraft position \mathbf{r}_0 ,
123 $\partial W_e(\mathbf{r}_0, t) / \partial t$.

124 3 Results

125 Twenty samples listed in Table 1, including sample 00 from Chen et al. (2019), were ana-
126 lyzed to seek the characteristic bipolar velocity-space signatures of electron Landau damping
127 and their evolution over time by varying the correlation interval τ . We evaluate the evolu-
128 tion of the electron energization with timestack plots of the parallel field-particle correlation
129 $C_{E_{\parallel}}(v_{\parallel}, t)$ over the sample duration in Figure 3(a) for sample 17 with $\tau = 3.96$ s and (c)

130 for sample 08 with $\tau = 1.98$ s. The time-averaged parallel correlations, taken over the full
 131 sample duration $\tau = T$, for these two intervals are plotted in (b) and (d). The timestack
 132 plots show that while the phase-space energy density transfer rate as a function of v_{\parallel} varies in
 133 time, when its amplitude is significant, it generally has the bipolar form characteristic of the
 134 Landau resonance about a parallel velocity $v_{\parallel}/v_{th,e} \sim 1$. Furthermore, the more clear bipo-
 135 lar velocity-space signatures in the time-averaged correlations, when looking at the timestack
 136 plots, are generally found to be more persistent in time.

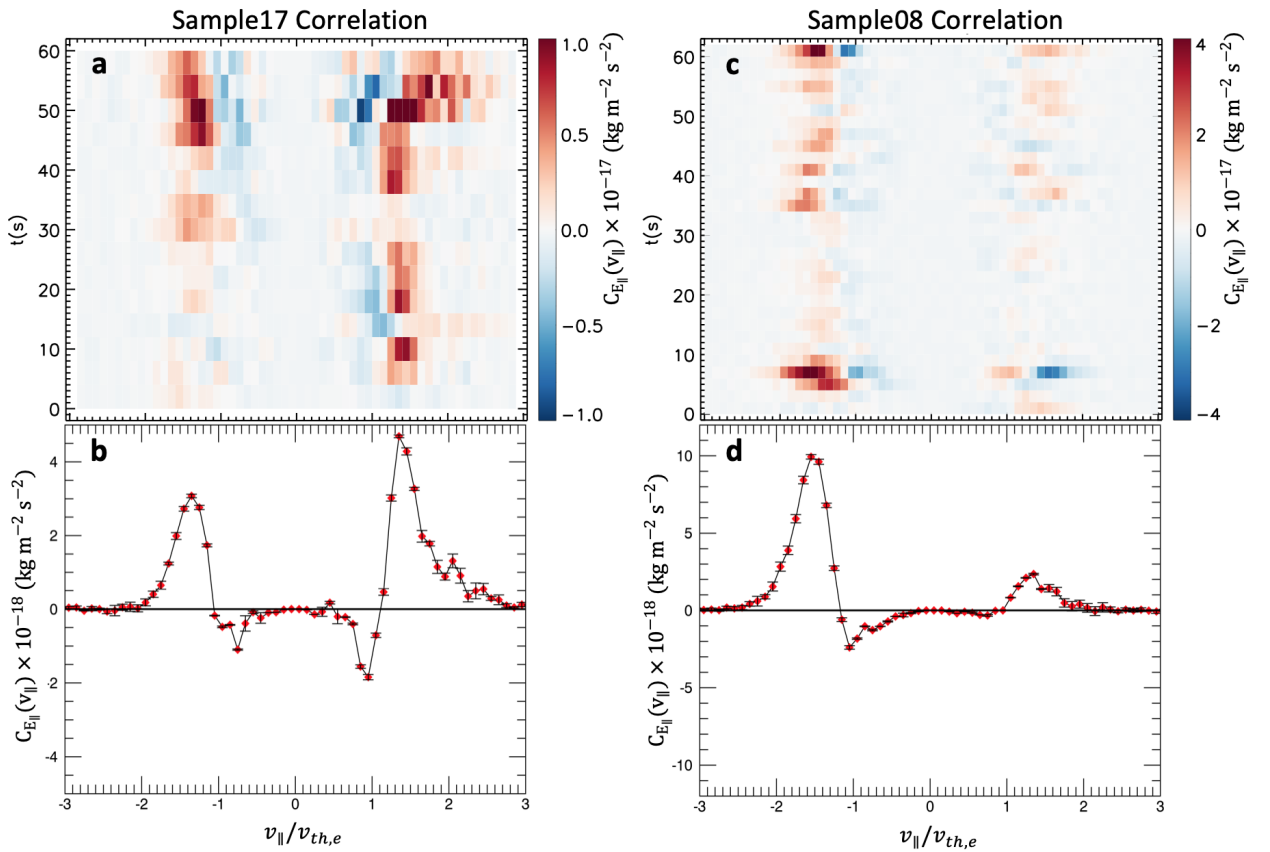


Figure 3: Timestack plots of $C_{E_{\parallel}}(v_{\parallel}, t)$ (a) for sample 17 with $\tau = 4$ s and (c) for sample 08 with $\tau = 2$ s and time-averaged correlation $C_{E_{\parallel}}(v_{\parallel})$ with $\tau = T$ for (b) sample 17 and (d) sample 08.

137 Linear kinetic theory predicts that, under the magnetosheath plasma parameters, the res-
 138 onant parallel phase velocities of KAWs generally satisfy $\omega/k_{\parallel}v_{th,e} = v_{\parallel}/v_{th,e} \sim 1$ when the
 139 collisionless damping becomes strong as $k_{\perp}\rho_e \rightarrow 1$. Therefore, the velocities of the zero
 140 crossings in the time-averaged, parallel velocity-space signatures correspond quantitatively to
 141 the resonant velocities expected for electron Landau damping.

142 In Figure 4, the time-averaged, parallel field-particle correlations $C_{E_{\parallel}}(v_{\parallel})$ for all twenty
 143 samples with $\tau = T$ are plotted. Five of the samples (05, 16, 17, 18, 19) show a velocity-space
 144 signature that is approximately symmetric about v_{\parallel} , qualitatively similar to sample 00 from
 145 Chen et al. (2019), but it appears that this result is not typical of all samples. However, all plots
 146 in Figure 4 but sample 09 show a clear bipolar velocity-space signature at either $v_{\parallel}/v_{th,e} \sim 1$
 147 or $v_{\parallel}/v_{th,e} \sim -1$, or both. Landau resonant damping of KAWs energizes particles moving
 148 approximately at the wave phase velocity *in the direction of wave propagation*, as illustrated
 149 in Figure 1. Therefore, we interpret the 13 examples of asymmetric velocity-space signatures
 150 in Figure 4 to indicate that more wave-energy flux is being damped in one-direction along \mathbf{B}_0
 151 than the other. In fact, a recent numerical simulation of the Chen et al. (2019) interval finds
 152 that the velocity-space signatures of electron Landau damping can have a variety of qualitative
 153 appearances (Horvath et al., 2020), similar to what is observed in Figure 4. In summary, it
 154 is found that 19 of the 20 intervals, representing 95% of the cases in Figure 4, show clear
 155 evidence that electron Landau damping is playing a key role in removing energy from the
 156 turbulent fluctuations in the magnetosheath.

With its ubiquity in magnetosheath turbulence established, the fraction of the turbulent
 dissipation governed by electron Landau damping is next identified. Integrating $C_{E_{\parallel}}(v_{\parallel})$ over
 v_{\parallel} yields the rate of change of electron spatial energy density due to E_{\parallel} at the point of ob-
 servation, $\partial W_e(\mathbf{r}_0, t)/\partial t$, with the results listed in Table 1. Note that, although the reversible
 nature of collisionless energy transfer allows for negative values that indicate the transfer of
 energy from electrons to E_{\parallel} , in all samples a net transfer of energy to the electrons is found.
 For each sample, this electron energization rate is compared with a theoretically estimated tur-

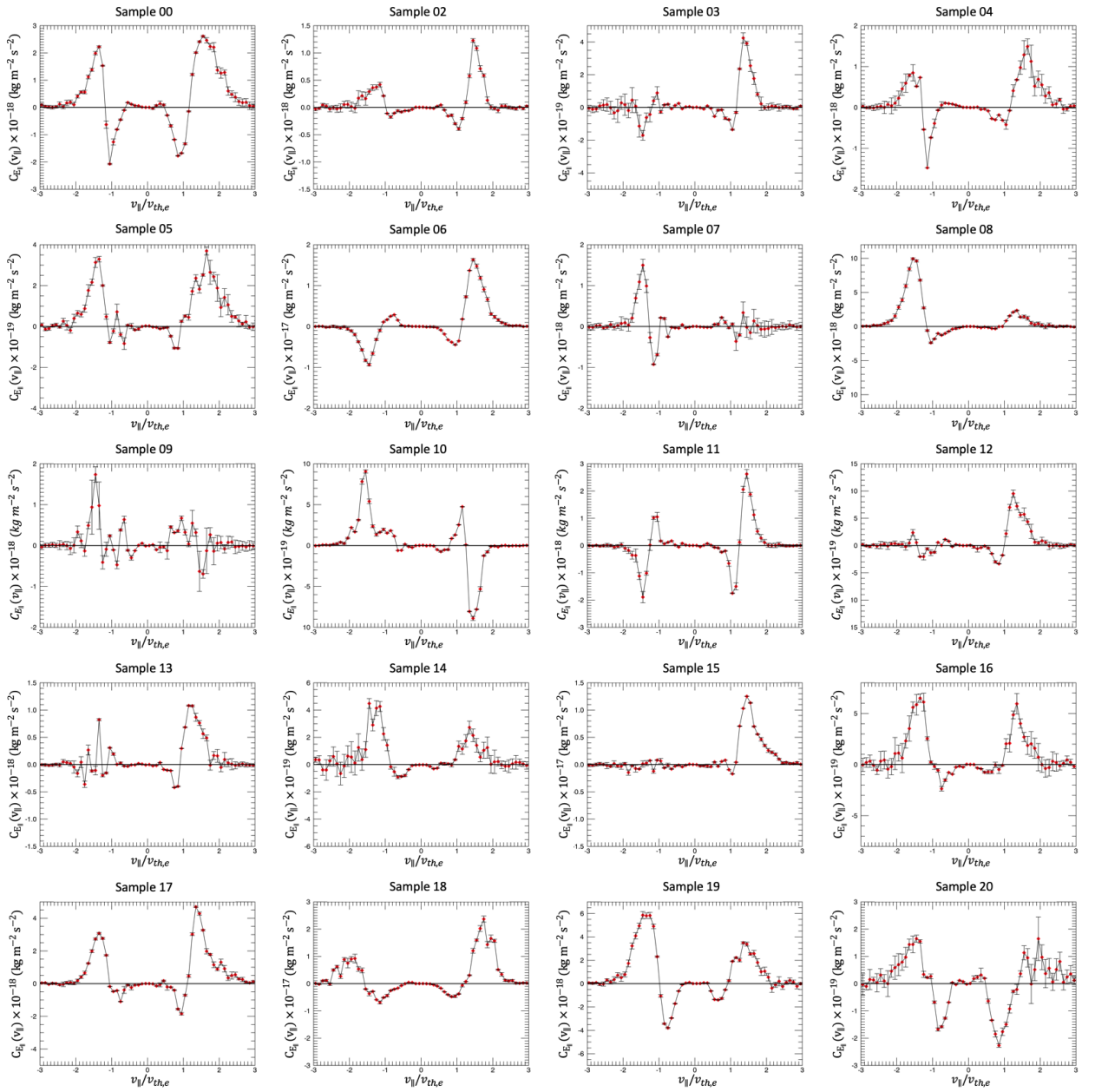


Figure 4: Time-averaged, parallel field-particle correlations $C_{E\parallel}(v_{\parallel})$ for all twenty samples with $\tau = T$ from Table 1.

bulent energy cascade rate ϵ in the inertial range from a cascade model (Howes et al., 2008, 2011) given by

$$\epsilon \sim \frac{\text{Energy Density}}{\text{Cascade Time}} = \frac{n_0 m_p U_{\perp}^2}{1/(k_{\perp} U_{\perp})} = n_0 m_p \left(\frac{2\pi f}{v_{\perp, sc}} \right) \frac{[\delta \hat{B}_{\perp}(f)]^3}{(\mu_0 n_0 m_p)^{3/2}}. \quad (6)$$

157 Here the turbulent energy density includes both kinetic and magnetic contributions which are
 158 assumed equal for Alfvénic turbulence, $\delta\hat{B}_\perp(f)$ is the amplitude of magnetic field fluctuations
 159 at the inertial range frequency $f = 0.2$ Hz computed from the time series as the increment
 160 with lag $t = 5$ s. The Taylor hypothesis (Taylor, 1938) is assumed to estimate k_\perp as the factor
 161 in parentheses where $v_{\perp,sc}$ is the component of the spacecraft velocity perpendicular to \mathbf{B}_0
 162 (Howes et al., 2014) and a typical anisotropy $k_\parallel \ll k_\perp$ is assumed (Sahraoui et al., 2010).
 163 The MHD Alfvén wave eigenfunction is used to estimate $U_\perp = \delta B_\perp v_A / B_0$. The resulting
 164 estimates for the turbulent energy cascade rate ϵ , listed in Table 1, are plotted against the
 165 measured electron energization rates $\partial W_e(\mathbf{r}_0, t) / \partial t$ in Figure 5.

166 The solid line in Figure 5 indicates $\partial W_e / \partial t = \epsilon$, meaning the measured rate of energiza-
 167 tion by electron Landau damping is sufficient to remove all of the energy from the turbulent
 168 cascade. Theoretically, however, the cascade rate estimate, derived from a scaling theory, is
 169 only an order-of-magnitude calculation, so dotted lines at factors of 3 above and below in-
 170 dicate the range of accuracy of this order-of-magnitude estimate for ϵ . Our key result is that
 171 nearly half of the samples have measured electron energization rates that fall within the order-
 172 of-magnitude estimate for ϵ , meaning that electron Landau damping is frequently a major, if
 173 not the dominant, mechanism responsible for the dissipation of turbulent energy in Earth’s
 174 magnetosheath.

175 4 Conclusion

176 An FPC analysis of a selection of twenty intervals of turbulence from the magnetosheath
 177 near the subsolar point has been performed to find that 95% of the intervals have velocity-
 178 space signatures of electron Landau damping. The resonant zero crossings of the bipolar
 179 velocity-space signatures are quantitatively consistent with the theoretical expectation for
 180 KAWs that the resonant phase velocities have values $\omega / k_\parallel v_{th,e} \sim 1$ as the collisionless damp-
 181 ing becomes strong. These findings confirm the first definitive identification of electron Lan-
 182 dau damping in the magnetosheath by Chen et al. (2019). However, it is found that only

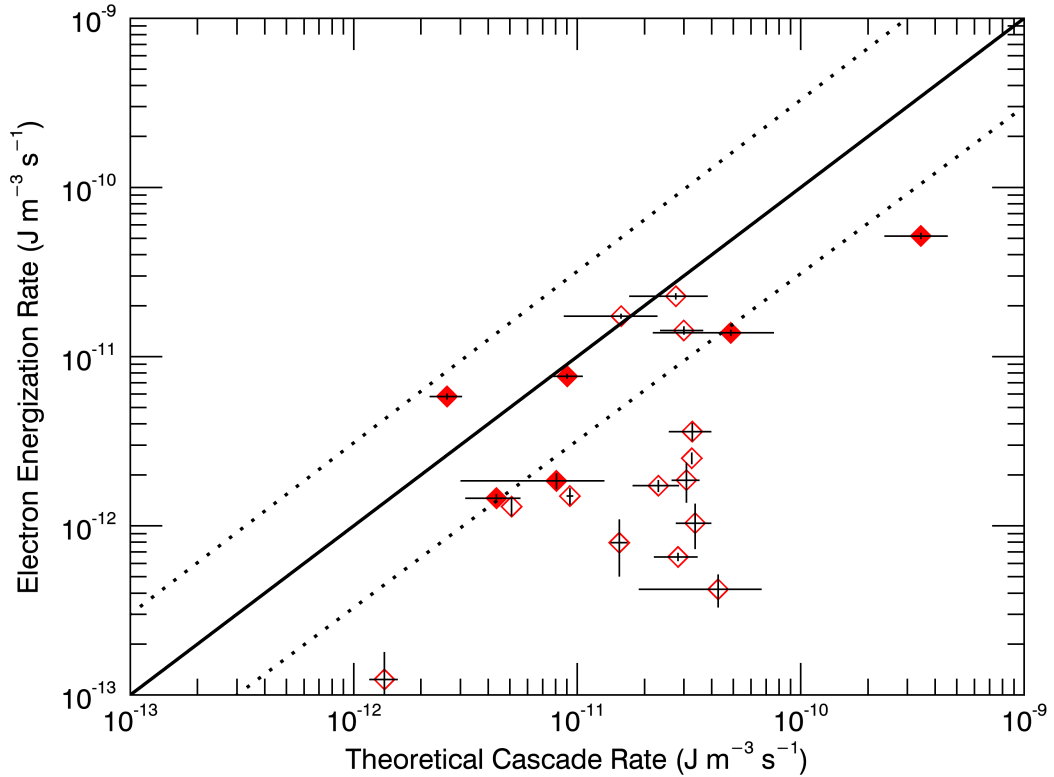


Figure 5: The electron energization rate $\partial W_e/\partial t$ vs. theoretical cascade rate ϵ , where the solid line indicates $\partial W_e/\partial t = \epsilon$ and the dotted lines indicate the range of the order-of-magnitude estimate of ϵ . Solid diamonds mark symmetric signatures, open diamonds asymmetric.

183 about one quarter of the intervals produce symmetric bipolar signatures at $v_{\parallel}/v_{th,e} \sim \pm 1$ as
 184 seen in Chen et al. (2019), indicating that typically one finds that the damping of waves in
 185 one direction along \mathbf{B}_0 exceeds that in the other direction, a finding consistent with a recent
 186 kinetic numerical simulation of magnetosheath turbulence (Horvath et al., 2020). Relative to
 187 the theoretically estimated turbulent energy cascade rate ϵ , it is found that nearly half of the
 188 samples have electron energization rates by Landau damping that account for the dissipation
 189 of a significant fraction, if not a majority, of the turbulent energy. In fact, the measured rates of
 190 electron energization by Landau damping span the range $\partial W_e/\partial t \in [10^{-13}, 10^{-11}] \text{ Jm}^{-3}\text{s}^{-1}$,

191 values that are much higher than the mean energy cascade rates of $\epsilon \lesssim 4 \times 10^{-14} \text{ Jm}^{-3}\text{s}^{-1}$ for
 192 Alfvénic cases and $\epsilon \lesssim 6 \times 10^{-13} \text{ Jm}^{-3}\text{s}^{-1}$ for magnetosonic cases reported in Hadid et al.
 193 (2018) for magnetosheath turbulence.

194 Future work will relax the restriction of the FPC analysis to intervals with relatively
 195 constant \mathbf{B}_0 and no velocity shears, enabling a larger statistical sample of MMS burst-mode
 196 intervals to be analyzed and to rule out selection bias in these results. In addition, the parallel
 197 Poynting energy flux will be examined in the cases with asymmetric signatures to test the
 198 interpretation that the wave damping is stronger for waves in one direction along \mathbf{B}_0 than the
 199 other.

200 **Acknowledgments**

201 This work was performed under the support of University of New Hampshire contract 06-
 202 0002 under NASA Prime contract NNG04EB99C. G. G. H. was supported by NASA grants
 203 80NSSC18K0643 and 80NSSC18K1371. A.S.A. would like to thank Jason Shuster and Tak
 204 Chu Li for the useful discussions. The data used in this research is available to the public via
 205 the MMS Science Data Center (<https://lasp.colorado.edu/mms/sdc/public/>).

206 **References**

- 207 Bruno, R., & Carbone, V. (2013, May). The Solar Wind as a Turbulence Laboratory. *Living*
 208 *Reviews in Solar Physics*, *10*(1), 2. doi: 10.12942/lrsp-2013-2
- 209 Chandran, B. D. G., Li, B., Rogers, B. N., Quataert, E., & Germaschewski, K. (2010,
 210 September). Perpendicular Ion Heating by Low-frequency Alfvén-wave Turbulence in
 211 the Solar Wind. , *720*(1), 503-515. doi: 10.1088/0004-637X/720/1/503
- 212 Chasapis, A., Retinò, A., Sahraoui, F., Vaivads, A., Khotyaintsev, Y. V., Sundkvist, D., ...
 213 Canu, P. (2015, May). Thin Current Sheets and Associated Electron Heating in
 214 Turbulent Space Plasma. , *804*(1), L1. doi: 10.1088/2041-8205/804/1/L1
- 215 Chen, C. H. K., Bale, S. D., Salem, C., & Mozer, F. S. (2011, August). Frame Depen-

- 216 dence of the Electric Field Spectrum of Solar Wind Turbulence. *Astrophys. J. Lett.*,
217 737, L41. doi: 10.1088/2041-8205/737/2/L41
- 218 Chen, C. H. K., Klein, K. G., & Howes, G. G. (2019, February). Evidence for electron Lan-
219 dau damping in space plasma turbulence. *Nature Communications*, 10, 740. doi: 10
220 .1038/s41467-019-08435-3
- 221 Cranmer, S. R., Asgari-Targhi, M., Miralles, M. P., Raymond, J. C., Strachan, L., Tian, H.,
222 & Woolsey, L. N. (2015, April). The role of turbulence in coronal heating and solar
223 wind expansion. *Philosophical Transactions of the Royal Society of London Series A*,
224 373(2041), 20140148-20140148. doi: 10.1098/rsta.2014.0148
- 225 Dobrowolny, M., & Torricelli-Ciamponi, G. (1985, January). Alfvén wave dissipation in the
226 solar wind. , 142(2), 404-410.
- 227 Ergun, R. E., Tucker, S., Westfall, J., Goodrich, K. A., Malaspina, D. M., Summers, D., ...
228 Cully, C. M. (2016, March). The Axial Double Probe and Fields Signal Processing
229 for the MMS Mission. , 199(1-4), 167-188. doi: 10.1007/s11214-014-0115-x
- 230 Hadid, L. Z., Sahraoui, F., Galtier, S., & Huang, S. Y. (2018, January). Compressible
231 Magnetohydrodynamic Turbulence in the Earth's Magnetosheath: Estimation of
232 the Energy Cascade Rate Using in situ Spacecraft Data. , 120(5), 055102. doi:
233 10.1103/PhysRevLett.120.055102
- 234 Hadid, L. Z., Sahraoui, F., Kiyani, K. H., Retinò, A., Modolo, R., Canu, P., ... Dougherty,
235 M. K. (2015, November). Nature of the MHD and Kinetic Scale Turbulence in the
236 Magnetosheath of Saturn: Cassini Observations. *Astrophys. J. Lett.*, 813(2), L29. doi:
237 10.1088/2041-8205/813/2/L29
- 238 Hollweg, J. V., & Markovskii, S. A. (2002). Cyclotron resonances of ions with obliquely
239 propagating waves in coronal holes and the fast solar wind. *Journal of Geo-*
240 *physical Research: Space Physics*, 107(A6), SSH 1-1-SSH 1-7. Retrieved from
241 [https://agupubs.onlinelibrary.wiley.com/doi/abs/10.1029/](https://agupubs.onlinelibrary.wiley.com/doi/abs/10.1029/2001JA000205)
242 2001JA000205 doi: 10.1029/2001JA000205

- 243 Hoppock, I. W., Chandran, B. D. G., Klein, K. G., Mallet, A., & Verscharen, D. (2018,
244 December). Stochastic proton heating by kinetic-Alfvén-wave turbulence in mod-
245 erately high- β plasmas. *Journal of Plasma Physics*, 84(6), 905840615. doi:
246 10.1017/S0022377818001277
- 247 Horvath, S. A., Howes, G. G., & McCubbin, A. J. (2020). Electron Landau Damping of Ki-
248 netic Alfvén Waves in Simulated Magnetosheath Turbulence. *Phys. Plasmas*. (submit-
249 ted)
- 250 Howes, G. G. (2017). A prospectus on kinetic heliophysics. *Phys. Plasmas*, 24(5), 055907.
251 doi: 10.1063/1.4983993
- 252 Howes, G. G., Cowley, S. C., Dorland, W., Hammett, G. W., Quataert, E., & Schekochihin,
253 A. A. (2008, May). A model of turbulence in magnetized plasmas: Implications
254 for the dissipation range in the solar wind. *Journal of Geophysical Research (Space
255 Physics)*, 113(A5), A05103. doi: 10.1029/2007JA012665
- 256 Howes, G. G., Klein, K. G., & Li, T. C. (2017, February). Diagnosing collisionless energy
257 transfer using field-particle correlations: Vlasov-Poisson plasmas. *J. Plasma Phys.*,
258 83(1), 705830102. doi: 10.1017/S0022377816001197
- 259 Howes, G. G., Klein, K. G., & TenBarge, J. M. (2014, July). Validity of the Taylor Hypothe-
260 sis for Linear Kinetic Waves in the Weakly Collisional Solar Wind. , 789(2), 106. doi:
261 10.1088/0004-637X/789/2/106
- 262 Howes, G. G., McCubbin, A. J., & Klein, K. G. (2018, February). Spatially lo-
263 calized particle energization by Landau damping in current sheets produced
264 by strong Alfvén wave collisions. *J. Plasma Phys.*, 84(1), 905840105. doi:
265 10.1017/S0022377818000053
- 266 Howes, G. G., Tenbarga, J. M., & Dorland, W. (2011, October). A weakened cascade model
267 for turbulence in astrophysical plasmas. *Physics of Plasmas*, 18(10), 102305-102305.
268 doi: 10.1063/1.3646400
- 269 Huang, S. Y., Hadid, L. Z., Sahraoui, F., Yuan, Z. G., & Deng, X. H. (2017, February).

- 270 On the Existence of the Kolmogorov Inertial Range in the Terrestrial Magnetosheath
271 Turbulence. , 836(1), L10. doi: 10.3847/2041-8213/836/1/L10
- 272 Johnson, J. R., & Cheng, C. Z. (2001, January). Stochastic ion heating at the magnetopause
273 due to kinetic Alfvén waves. , 28(23), 4421-4424. doi: 10.1029/2001GL013509
- 274 Kiyani, K. H., Osman, K. T., & Chapman, S. C. (2015, April). Introduction: Dissipation and
275 heating in solar wind turbulence: from the macro to the micro and back again. *Philosophical Transactions of the Royal Society of London Series A*, 373, 40155.
276
- 277 Klein, K. G., & Howes, G. G. (2016, August). Measuring Collisionless Damping in Helio-
278 spheric Plasmas using Field-Particle Correlations. *Astrophysical Journal Letters*, 826,
279 L30. doi: 10.3847/2041-8205/826/2/L30
- 280 Klein, K. G., Howes, G. G., & Tenborge, J. M. (2017, August). Diagnosing collisionless
281 energy transfer using field-particle correlations: gyrokinetic turbulence. *Journal of*
282 *Plasma Physics*, 83(4), 535830401. doi: 10.1017/S0022377817000563
- 283 Klein, K. G., Howes, G. G., TenBerge, J. M., & Valentini, F. (2020). Diagnosing collision-
284 less energy transfer using field-particle correlations: Alfvén-ion cyclotron turbulence.
285 *Journal of Plasma Physics*, 86, 905860402. doi: 10.1017/S0022377820000689
- 286 Leamon, R. J., Smith, C. W., Ness, N. F., & Wong, H. K. (1999). Dissipation range dynam-
287 ics: Kinetic alfvén waves and the importance of e . *Journal of Geophysical Research:*
288 *Space Physics*, 104(A10), 22331-22344. Retrieved from [https://agupubs](https://agupubs.onlinelibrary.wiley.com/doi/abs/10.1029/1999JA900158)
289 [.onlinelibrary.wiley.com/doi/abs/10.1029/1999JA900158](https://agupubs.onlinelibrary.wiley.com/doi/abs/10.1029/1999JA900158) doi:
290 10.1029/1999JA900158
- 291 Lindqvist, P. A., Olsson, G., Torbert, R. B., King, B., Granoff, M., Rau, D., ... Tucker, S.
292 (2016, March). The Spin-Plane Double Probe Electric Field Instrument for MMS. ,
293 199(1-4), 137-165. doi: 10.1007/s11214-014-0116-9
- 294 Martinović, M. M., Klein, K. G., Kasper, J. C., Case, A. W., Korreck, K. E., Larson, D., ...
295 MacDowall, R. J. (2020, February). The Enhancement of Proton Stochastic Heating
296 in the Near-Sun Solar Wind. , 246(2), 30. doi: 10.3847/1538-4365/ab527f

- 297 Pollock, C., Moore, T., Jacques, A., Burch, J., Gliese, U., Saito, Y., . . . Zeuch, M. (2016,
298 March). Fast Plasma Investigation for Magnetospheric Multiscale. , *199*(1-4), 331-
299 406. doi: 10.1007/s11214-016-0245-4
- 300 Ruhunusiri, S., Halekas, J. S., Espley, J. R., Mazelle, C., Brain, D., Harada, Y., . . . Howes,
301 G. G. (2017, January). Characterization of turbulence in the Mars plasma environ-
302 ment with MAVEN observations. *Journal of Geophysical Research (Space Physics)*,
303 *122*(1), 656-674. doi: 10.1002/2016JA023456
- 304 Russell, C. T., Anderson, B. J., Baumjohann, W., Bromund, K. R., Dearborn, D., Fischer,
305 D., . . . Richter, I. (2016, March). The Magnetospheric Multiscale Magnetometers. ,
306 *199*(1-4), 189-256. doi: 10.1007/s11214-014-0057-3
- 307 Sahraoui, F., Goldstein, M. L., Belmont, G., Canu, P., & Rezeau, L. (2010, Septem-
308 ber). Three Dimensional Anisotropic k Spectra of Turbulence at Subproton
309 Scales in the Solar Wind. *Phys. Rev. Lett.*, *105*(13), 131101. doi: 10.1103/
310 PhysRevLett.105.131101
- 311 Schekochihin, A. A., Cowley, S. C., Dorland, W., Hammett, G. W., Howes, G. G., Quataert,
312 E., & Tatsuno, T. (2009, May). ASTROPHYSICAL GYROKINETICS: KINETIC
313 AND FLUID TURBULENT CASCADES IN MAGNETIZED WEAKLY COLLI-
314 SIONAL PLASMAS. *The Astrophysical Journal Supplement Series*, *182*(1), 310–377.
315 Retrieved from [https://doi.org/10.1088%2F0067-0049%2F182%2F1%
316 2F310](https://doi.org/10.1088%2F0067-0049%2F182%2F1%2F310) doi: 10.1088/0067-0049/182/1/310
- 317 Tao, C., Sahraoui, F., Fontaine, D., Patoul, J., Chust, T., Kasahara, S., & Retinò, A. (2015,
318 April). Properties of Jupiter’s magnetospheric turbulence observed by the Galileo
319 spacecraft. *Journal of Geophysical Research (Space Physics)*, *120*(4), 2477-2493. doi:
320 10.1002/2014JA020749
- 321 Taylor, G. I. (1938). The Spectrum of Turbulence. *Proc. Roy. Soc. A*, *164*, 476–490.
- 322 Tu, C. Y., & Marsch, E. (1995). *MHD structures, waves and turbulence in the solar wind:
323 observations and theories.*

- 324 von Papen, M., Saur, J., & Alexandrova, O. (2014, April). Turbulent magnetic field fluctu-
325 ations in Saturn's magnetosphere. *Journal of Geophysical Research (Space Physics)*,
326 *119*(4), 2797-2818. doi: 10.1002/2013JA019542
- 327 Vörös, Z., Yordanova, E., Echim, M. M., Consolini, G., & Narita, Y. (2016). Turbulence-
328 generated Proton-scale Structures in the Terrestrial Magnetosheath. , *819*(1), L15. doi:
329 10.3847/2041-8205/819/1/L15